Published in final edited form as:
Mol Cancer Ther. 2013 December ; 12(12): . doi:10.1158/1535-7163.MCT-13-0204.

Urokinase Plasminogen Activator System Targeted Delivery of Nanobins as a Novel Ovarian Cancer Therapeutics

Yilin Zhang[1], **Hilary A. Kenny**[1], **Elden P. Swindell**[2,3], **Anirban K. Mitra**[1], **Patrick L. Hankins**[2,4], **Richard W. Ahn**[2,4], **Katja Gwin**[5], **Andrew P. Mazar**[2,6,7], **Thomas V. O'Halloran**[2,4,7], and **Ernst Lengyel**[1,8]

[1]Department of Obstetrics and Gynecology/Section of Gynecologic Oncology, University of Chicago, Chicago, Illinois

[2]Chemistry of Life Processes Institute, Northwestern University, Evanston, Illinois

[3]Department of Chemical and Biological Engineering, Northwestern University, Evanston, Illinois

[4]Department of Chemistry, Northwestern University, Evanston, Illinois

[5]Department of Pathology, University of Chicago, Chicago, Illinois

[6]Department of Molecular Biosciences, Northwestern University, Evanston, Illinois

[7]Robert H. Lurie Comprehensive Cancer Center, Northwestern University, Evanston, Illinois

Abstract

The urokinase system is overexpressed in epithelial ovarian cancer (OvCa) cells and is expressed at low levels in normal cells. To develop a platform for intracellular and targeted delivery of therapeutics in OvCa, we conjugated urokinase plasminogen activator (uPA) antibodies to liposomal nanobins. The arsenic trioxide loaded nanobins had favorable physicochemical properties and the ability to bind specifically to uPA. Confocal microscopy showed that the uPA targeted nanobins were internalized by OvCa cells, while both ICP-MS and FACS analyses confirmed >4-fold higher uptake of targeted nanobins when compared to untargeted nanobins. In a co-culture assay, the targeted nanobins showed efficient uptake in OvCa cells but not in the normal primary omental mesothelial cells. Moreover, this uptake could be blocked by either down-regulating uPA receptor expression in the OvCa cells using shRNA or by competition with free uPA or uPA antibody. In proof-of-concept experiments, mice bearing orthotopic ovarian tumors showed a greater reduction in tumor burden when treated with targeted nanobins than with untargeted nanobins (47% *versus* 27%; $p<0.001$). The targeted nanobins more effectively inhibited tumor cell growth both *in vitro* and *in vivo* compared to untargeted nanobins, inducing caspase-mediated apoptosis and impairing stem cell marker, ALDH1A1, expression. *Ex vivo* fluorescence

[8]Corresponding author: Ernst Lengyel, Department of Obstetrics and Gynecology, University of Chicago (MC 2050), 5841 South Maryland Avenue, Chicago, IL 60637; elengyel@uchicago.edu.

Conflict of Interest: Andrew Mazar and Thomas O'Halloran own equity in and receive consulting fees from Tactic Pharma, which owns the ATN-291 antibody. Thomas O'Halloran has an issued patent on the arsenic-containing nanobins. The other authors have declared no COI.

Authors' Contributions

Conception and Design: H.A. Kenny, A.P. Mazar, T.V. O'Halloran, E. Lengyel
Experiments: Y. Zhang, H.A. Kenny, E.P. Swindell, P.L. Hankins, A.K. Mitra
Development of methodology: E.P. Swindell, P.L. Hankins, Y. Zhang, H.A. Kenny, R.W. Ahn, T.V. O'Halloran, A.P. Mazar
Immunohistochemistry: K. Gwin
Analysis and interpretation of data: Y. Zhang, H.A. Kenny, E.P. Swindell, P.L. Hankins, A.K. Mitra, R.W. Ahn, K. Gwin, A.P. Mazar, T.V. O'Halloran, E. Lengyel
Study supervision: E. Lengyel

imaging of tumors and organs corroborated these results, showing preferential localization of the targeted nanobins to the tumor. These findings suggest that uPA targeted nanobins capable of specifically and efficiently delivering payloads to cancer cells could serve as the foundation for a new targeted cancer therapy utilizing protease receptors.

Keywords

ovarian cancer; drug delivery; urokinase; urokinase receptor; nanobin

Introduction

Ovarian cancer (OvCa), which usually presents at an advanced clinical stage, is the most aggressive gynecological malignancy, accounting for 6% of all cancer-related deaths in women in the United States (1). The most common sites of OvCa metastasis are the other ovary, the peritoneum, and the omentum, while distant, extra-abdominal metastases are rare (2, 3). The current standard of care includes debulking surgery and subsequent adjuvant chemotherapy with taxane and platinum-containing drugs. This chemotherapy combination clearly prolongs the lives of OvCa patients; however, almost all tumors will eventually become chemoresistant (1).

Unfortunately, no new drugs have been approved for the treatment of OvCa since 1999, when liposomal doxorubicin (Doxil®) was introduced for the treatment of recurrent disease. Doxil®, when compared to free doxorubicin, has a longer half-life due to its encapsulation in a poly(ethylene glycol) (PEG) coated liposome (4). The small size of the Doxil® particles (≈100 nm) increases drug accumulation by escape through fenestrated tumor vasculature. The favorable clinical pharmacokinetics and toxicity profile of Doxil®, which causes less cardiotoxicity and nausea than doxorubicin (5), has contributed to its clinical efficacy in recurrent OvCa. Doxil® represents one of the first examples of the successful transfer of nanotechnology into the clinical setting based on a rationale developed using a human OvCa tumor xenograft model (4, 6) and sets a precedent for liposomal delivery as a means to deliver cancer drugs with more efficacy and fewer side effects (7, 8).

For nanoparticles to reach their full potential in cancer therapy, they should be designed with reduced off-target toxicity and increased circulation half-life for improved passive tumor uptake. These particles should ideally utilize a cancer cell-targeted delivery method to specifically deliver large doses of a therapeutic payload directly into tumor cells. Indeed, nanoparticles can be modified for tumor cell-specific delivery with cancer-targeting ligands such as antibodies (9), aptamers (10), peptides (11), or folate (12) that recognize receptors or antigens overexpressed on the surface of cancer cells. There are particular advantages to using antibodies for targeting. These include ease of conjugation, high target specificity and the potential for antibody-directed cellular cytotoxicity (13).

In our search for new treatments for women's cancer, we had previously encapsulated arsenic trioxide (As_2O_3, As), an FDA-approved drug for acute promyelocytic leukemia, into nanoparticles. This novel formulation strategy allowed encapsulation of a high concentration of As in a stable precipitate with nickel acetate (Ni) that we designated as a nanobin (Ni, As) (12, 14, 15). We showed that these nanobins significantly inhibited tumor cell growth in an orthotopic triple negative human breast cancer xenograft model (14). However, the poor pharmacokinetic profile of As_2O_3, including a short plasma half-life and dose-limiting toxicity, had prevented its development for solid tumor indications (16, 17). The nanobin formulation of As_2O_3 resolved these issues, resulting in increased tumor accumulation, activity, plasma half-life and improved tolerability when compared to free As_2O_3 (12, 14).

To further improve anti-tumor activity, we conjugated an antibody raised against the urokinase plasminogen activator (uPA) (ATN-291) to the arsenic nanobins (18). Both uPA and its receptor, u-PAR, are highly expressed in epithelial tumors (19) including OvCa, where it is detected in as many as 90% of clinical OvCa specimens but not in untransformed ovarian/tubal epithelium (summarized in Kenny et al. (20)). The antibody, ATN-291, binds to the kringle domain of uPA, even when it is bound to u-PAR, and the entire complex is internalized (18). Because uPA is internalized as a complex (21, 22) we reasoned that an antibody against uPA conjugated to nanobins would bind to tumor cells displaying receptor-bound or soluble uPA and, by leading to the internalization of the nanobin/uPA/u-PAR complex, results in intracellular delivery of a large arsenic payload.

In this study, we explore the hypothesis that targeting a nanobin formulation of As_2O_3 to the uPA system that is highly expressed in OvCa will improve the drug's antitumor activity. The targeted nanobin formulation may revive the development of a promising cancer drug by combining specific delivery with improved pharmacokinetics. We report here that the targeted nanobins internalize into u-PAR-expressing cancer cells, and effectively impair OvCa tumor growth.

Materials and Methods

Reagents and cell lines

Antibodies against u-PAR (ATN-658 for immunoblot, and ATN-615 for immunohistochemistry) and the uPA antibody ATN-291 were manufactured by SDIX (Newark, DE) (18), while antibody (UK-1) for immunoblot was from American Diagnostica Inc. (Stamford, CT). ALDH1A1 (B-5) antibody was obtained from Santa Cruz (Santa Cruz, CA). Cleaved caspase 3 (Asp175) and GAPDH (14C10) antibodies were from Cell Signaling (Danvers, MA), and MMP-2 (IM33) antibody was from Millipore (Billerica, MA). Hoechst 33342 and JC-1 dye were purchased from Invitrogen (Carlsbad, CA). Collagen type I (rat-tail), was purchased from BD Bioscience (Bedford, MA) and 1,2-distearoyl-sn-glycero-3-phosphocholine (DSPC), and 1,2-distearoyl-sn-glycero-3-phosphoethanolamine-N-[amino(polyethyleneglycol)-2000] (DSPE-PEG_{2000}) were from Avanti Polar Lipids (Alabaster, AL). Cell culture grade endotoxin free water was from Thermo Scientific. Arsenic Trioxide (As_2O_3), nickel (II) acetate, cholesterol, and other chemical reagents were purchased from Sigma-Aldrich (St. Louis, MO) unless otherwise indicated.

The CaOV3 and ES-2 human ovarian cancer cell lines were from ATCC (American Type Culture Collection, Manassas, VA). SKOV3ip1 and HeyA8 cells were provided by Dr. Gordon Mills (M.D. Anderson Cancer Center, Houston, TX). All human OvCa cell lines (HeyA8, SKOV3ip1, ES-2, CaOV3) and the primary OvCa clone MONTY-1 were maintained in Dulbecco's modified Eagle's medium (DMEM, Invitrogen). MONTY-1 was isolated from human omental metastases and used at an early passage (23). All cell lines were validated by short tandem repeat (STR) DNA fingerprinting using the AmpFℓSTR Identifier kit (Applied Biosystems). The STR profiles were compared to known ATCC fingerprints, to the Cell Line Integrated Molecular Authentication database (CLIMA), and to the MD Anderson fingerprint database.

Preparation of alkyne-functional nanobins

Arsenic/nickel complex loaded nanobins, NB(Ni,As), and empty nanobin controls NB(NaCl) were prepared and described in supplementary materials and methods as previously reported (14, 18). DSPE-PEG_{3400}-NH_2 (Laysan Bio) was reacted with 4-pentynoic acid in the presence of 1-ethyl-3-(3-dimethylaminopropyl) carbodiimide (EDC) and n-NHS in chloroform at 60°C overnight. The resulting alkyne-functional lipid (DSPE-

PEG_{3400}-Alkyne) was dried, dissolved in deionized water, and lyophilized. The DSPE-PEG_{3400}-Alkyne lipid was then incubated with preformed nanobins at a DSPE-PEG_{3400}-Alkyne to nanobin phospholipid molar ratio of 0.01 for 1 h at 60°C, allowing it to insert into the lipid bilayer. Meanwhile, the total arsenic content of the nanobin solution was adjusted to 25 mM to ensure that the drug loading does not change during heating. The alkyne functional nanobins were purified by diafiltration against 20 mM HEPES and 150 mM NaCl, pH 7.4. The phospholipid, arsenic and nickel molar concentrations were then measured by ICP-OES.

Preparation of urokinase antibody conjugated nanobins

The uPA Ab (ATN-291) was conjugated to the surface of the nanobins using a copper(I)-catalyzed azide-alkyne cycloaddition reaction (24). The alkyne-functionalized nanobins described above were incubated with the azide-functionalized AlexaFluor647-labeled ATN-291 at a molar ratio of 3×10^{-4} moles antibody per mole of phospholipid. The preparation of azide-functionalized AlexaFluor647-labeled ATN-291 was described in supplementary materials and methods. Copper (II) sulfate, tris(3-hydroxypropyltriazolylmethyl) amine, and sodium ascorbate were added to the reaction mixture to a final concentration of 200 μM, 1 mM and 2 mM, respectively. The reaction proceeded for 90 minutes at 37°C, when fresh sodium ascorbate was added, bringing the total concentration to 3 mM. The reaction continued for an additional 90 minutes at 37°C. The unconjugated antibody was removed from the solution using diafiltration against 20 mM HEPES and 150 mM NaCl, pH 7.4.

Quantification of nanobin conjugated antibodies

The number of uPA antibodies conjugated per nanobin was determined by UV/Vis after proteolysis. Urokinase antibody conjugated nanobins were incubated with 4 mg/mL of pronase for 2h at 37°C. Digested antibody was then separated from intact nanobins using an Amicon Ultra spin filter (50k MWCO, Millipore). The concentration of AF647-labeled ATN-291 was determined by measuring absorbance at 650 nm with a spectrophotometer (Perkin Elmer) and was used as a proxy for ATN-291 concentration.

Transmission electron microscopy

Nanobins were visualized using the negative staining technique via a TECNAI F30 transmission electron microscope (FEI Company). The nanobin suspension was dropped onto a glow-discharged carbon-coated copper grid and stained with 1% uranyl acetate. Images were examined under 300KV with Gatan CCD digital micrograph (25).

Dynamic light scattering (DLS) and zeta potential

The measurement of hydrodynamic size and polydispersity index (PDI) of nanobins was performed using a 384-well microplate reader using a DynaPro Nanostar (Wyatt Technology Corporation, Santa Barbara, CA). The zeta potential assessment was carried out in a clear disposable zeta cell using a Zetasizer Nano ZS analyzer (Malvern Instruments Ltd, Worcestershire, UK). Both DLS and zeta potential were performed in PBS at 25°C, and the results were the average of at least 10 measurements from 3 independent batches.

Inductively-coupled plasma-optical emission spectroscopy and -mass spectrometry

For ICP-OES, all nanobin samples and standards were prepared in a matrix composed of deionized water, 3% nitric acid, 2% acetic acid, 0.1% triton x-100, and 0.5 parts per million (ppm) indium internal standards. Known quantitative standards were prepared at concentrations ranging from 0.50 to 10 ppm arsenic, nickel, and phosphorous. A matrix only standard was also included.

For ICP-MS, the tissues were rinsed with PBS and frozen at −80°C until analysis. For elemental biodistribution, frozen tissues were submerged in concentrated nitric acid, and digested in a Milestone EthosEZ microwave digestion system. Samples and standards were then diluted into an ultrapure deionized water matrix containing 3% nitric acid, 2% acetic acid, 0.1% Triton X-100, containing 5 parts per billion (ppb) indium as an internal standard.

Immunohistochemistry

Slides containing human OvCa tissue were deparaffinized. The u-PAR was detected with a primary antibody (ATN-615, 1:200) and imaged through an avidin-biotin-free detection system (Dako Envision) (20, 26). For HeyA8 xenograft tumors, a representative tumor area was first confirmed by a gynecologic pathologist (KG). Immunohistochemical staining of mouse tumor sections were performed to assess markers of apoptosis (cleaved caspase 3, Asp175, 1:20), and OvCa stem cell markers (ALDH1A1, B5, 1:400). Terminal deoxynucleotidyl transferase-mediated deoxyuridine triphosphate nick end labeling (TUNEL) was performed using the ApopTag® Plus Peroxidase *In Situ* Apoptosis Kit (Millipore). The stained cells were imaged at 100× and 400× magnification from five random fields (25), and quantified by NIH ImageJ software. Immunohistochemical staining of microvessel density (CD31, M-20, 1:50), proliferation (Ki67, SP6, 1:300) and the mouse macrophage (F4/80, A3-1, 1:500) was described in supplementary materials and methods.

Immunoblot

Immunoblot was performed as previously described (20, 26). The following antibodies were used: uPA (UK-1, 1:1000), u-PAR (ATN-658, 1:2000), cleaved caspase 3 (Asp175, 1:1000), ALDH1A1 (B-5, 1:250), MMP-2 (IM33, 1:1000) and GAPDH (14C10, 1:1000). For cytotoxicity studies, the HeyA8 cells were treated for 1 day with NB(Ni,As) (200 μM of As), ATN-291-NB(Ni,As) (200 μM of As), As_2O_3 (20 μM of As), or ATN-291-NB(NaCl).

Confocal microscopy

Cells were cultured for 3 days and then treated with nanobins (25 μM, lipid concentration). To evaluate internalization, Z-stack scanning was performed by adjusting the focal plane from the bottom to the top of the cells, followed by orthogonal 3-dimensional projection. For the OvCa cell–targeted delivery study, primary human mesothelial cells isolated from omentum of patients (27) were co-cultured with HeyA8-GFP cells and were treated with ATN-291_{AF647}-NB(Ni,As) for 24 h. For apoptosis assessment, HeyA8 cells were treated with 25 μM of arsenic trioxide, NB(Ni,As), or ATN-291-NB(Ni,As) for 2 h to measure mitochondrial membrane potential with the JC-1 dye, or for 18 h to measure DNA fragmentation with Hoechst. Staining was done with 2 μM of JC-1 or 4 μM of Hoechst 33342 dyes for 30 min, respectively. The images were acquired with a Leica SP5 confocal laser scanning microscope (oil lens-63×/1.4N). The excitation and emission wavelengths were set for the detection of JC-1 aggregates (488/514 nm), JC-1 monomer (561/592 nm), AF647 (633/650 nm), and Hoechst (360/450 nm).

Flow cytometry

OvCa cancer cells were treated with 25 μM (lipid concentration) of ATN-291-NB(Calcein) or NB(Calcein). For time-course studies, HeyA8 cells were monitored over 1–48 h. In competition assays, HeyA8 cells were pre-treated with either ATN-291 or single chain uPA (scuPA) with the indicated concentrations for 2 h before further incubation with nanobins for 24 h. In receptor-competition assays, ES-2 WT and KD cells were incubated with nanobins for 24 h. After incubation, cells were washed, detached, resuspended in PBS, fixed by 2% paraformaldehyde, and stored at 4°C until analysis. A total of 10,000 events were collected for each sample using an LSRFortessa cell analyzer (calcein: 488/515 nm,

Alexa647: 641/670 nm). Data were analyzed by FlowJo software (TreeStar Inc). The analysis of JC-1 stained cells was described in supplementary materials and methods.

Animal studies

Hey8-GFP (5×10^5) cells (28) were injected intraperitoneally (i.p.) into 5–6 week-old athymic female nude mice. Four days post inoculation, the mice were randomized into 5 groups (5 mice/group): 200 μL of As_2O_3, NB(Ni,As), ATN-291-NB(Ni,As), PBS or ATN-291-NB(NaCl) were injected i.p. and injections repeated 5 times every other day at arsenic concentration of 4 mg/kg (14). The mice were dissected two days after the last treatment. All animal experiments described were approved by IACUC. To study nanobin biodistribution, organs (liver, heart, lung, spleen, kidney) and the tumor were dissected, rinsed with PBS, and imaged using an Olympus fluorescence molecular imaging system. Blood toxicity studies were described in supplementary materials and methods.

Cell fractionation

HeyA8 cells treated with nanobins for 24 h followed by fractionation using the Qproteome cell compartment kit (Qiagen, Valencia, CA). The cell compartments were isolated according to the manufacturer's instructions. The cytosolic, membrane/organelle, and nuclear compartments were verified by immunoblot before ICP-MS analysis for arsenic content.

Statistical analysis

Results were analyzed as means ± SEM. Statistical analyses were performed using two-tailed *t*-test or one-way ANOVA at $p<0.05$ level of significance with Graphpad Prism version 5.04 (La Jolla, CA). The TCGA database was queried for u-PAR expression in 580 OvCa patients (29) and analyzed using the cBio cancer genomics portal (http://www.cbioportal.org/public-portal/index.do) (30).

Results

Synthesis and characterization of urokinase antibody conjugated nanobins loaded with arsenic trioxide

Epithelial OvCa cells homogeneously express elevated levels of u-PAR in the primary tumor and all abdominal metastasis (Fig. 1A). Analysis of the TCGA OvCa database (29) at the cBio cancer genomics portal (30) showed that OvCa patients with u-PAR gene expression alterations had a significantly worse overall (19.5 *versus* 44.3 months) and disease-free survival (12.0 *versus* 17.5 months) (Supplementary Fig. S1A). And our previous tissue microarray studies demonstrated that u-PAR is highly expressed in epithelial tumors (19) including > 90% of clinical OvCa specimens (20). This raises the possibility that high u-PAR expression might not only function as a marker of aggressiveness for epithelial OvCa cells but could also be used to specifically deliver a therapeutic payload to those cells. For the experiments described below, we identified OvCa cell lines with high (HeyA8, ES-2) and with low (SKOV3ip1, MONTY-1, and CaOV3) u-PAR expression, all of which also express uPA (Fig. 1B). Since the uPA system is highly expressed in OvCa (18, 20, 31), we sought to develop novel nanobins that would actively target uPA/u-PAR expressing OvCa cells. A monoclonal antibody raised against the kringle domain of uPA in mice (ATN-291) was chosen as a targeting ligand since it binds tightly to human uPA with a $K_d\approx0.5$ nM and does not disrupt uPA/u-PAR binding (18). The nanobins were assembled from cholesterol, DSPC, and DSPE-PEG, and loaded with an arsenic/nickel co-precipitate (Fig. 1C, Supplementary Fig. S1B) (12, 14, 15). Next, DSPE-PEG-Alkyne was post-inserted into the bilayer to facilitate the conjugation of the azide-functionalized uPA antibody using

click chemistry. This method ensures that the targeting antibodies are not exposed to potentially denaturing high-temperatures (Fig. 1C) (32). To facilitate characterization of antibody-nanobin conjugates, the antibody was labeled with AlexaFluor647 (AF647) prior to click chemistry. UV/Vis analysis of AF647 after proteolysis showed that the arsenic-loaded nanobins were decorated with an average of 8.5 antibodies per nanobin (Table 1). We also found that, after conjugation, the ATN-291 targeted nanoparticle still bound uPA with nanomolar binding affinity (data not shown).

The lipid composition of the nanobins was optimized to ensure that the nanobin surface was neutral at physiological pH and to minimize non-specific cellular binding. The conjugation of ATN-291 to the nanobin minimally affected the neutral zeta potential of the lipid membrane (Fig. 1D, Table 1). Dynamic light scattering (DLS) was applied to assess the hydrodynamic diameter and polydispersity of the nanoparticles before and after antibody conjugation. The average hydrodynamic diameter of the arsenic loaded ATN-291-NB(Ni,As) was 104.4 nm, an increase of 10.5% when compared to NB(Ni,As) (94.4 nm), which was expected given the addition of antibodies. Although the conjugation of the uPA-antibody to NB(Ni,As) may increase the heterogeneity of the nanoparticle, the polydispersity index of ATN-291-NB(Ni,As) remained low (Fig. 1E, Table 1). Transmission electron microscopy also showed that the antibody conjugated nanobins are homogenous, spherical particles (Fig. 1F).

Cellular uptake of the urokinase antibody conjugated nanobins are urokinase and urokinase receptor dependent

Binding of uPA to u-PAR triggers internalization (21). To determine if the antibody conjugated nanobins are internalized we made (i) calcein encapsulated nanobins to visualize if the nanobin payload becomes internalized into the cytoplasm (Fig. 2A, B), and (ii) ATN-291AF647-nanobins, with the antibody labeled with AF647, to evaluate whether the antibody is internalized together with the nanobins (Fig. 2C–E).

Confocal microscopy showed strong calcein fluorescence in the cytoplasm of HeyA8 cells treated with ATN-291-NB(Calcein) at both 3 h and 24 h time points, while the uptake of untargeted NB(Calcein) was much lower (Fig. 2A). This was confirmed in flow cytometry studies in which, after 24 h, HeyA8 cells treated with ATN-291-NB(Calcein) showed a 4-fold higher mean fluorescence intensity (MFI) compared to NB(Calcein), confirming effective cellular uptake of nanobins targeted to uPA (Fig. 2B). The uptake of fluorescently labeled ATN-291_{AF647}-NB(Ni,As) was increased in HeyA8 cells in a time-dependent manner with maximal signal after incubation for 24 h (Fig. 2B, C). Confocal laser scanning microscopy showed cytoplasmic localization of ATN-291_{AF647}-NB(Ni,As) when single micron optical sections were reassembled in 3D and the reconstruction shown from the side to visualize the entire Z-axis (Fig. 2D). After only 6 h, most of the ATN-291_{AF647}-NB(Ni,As) was detected in a perinuclear position, shown previously to be caused by u-PAR internalization (22). Specificity of the targeted nanobins could also be shown by co-culturing primary human mesothelial cells with GFP expressing OvCa cells (Fig. 2E). The AF647 labeled antibody (red) co-localized with the high u-PAR expressing OvCa cells (green) but was not detected in the u-PAR negative mesothelial cells (Fig. 2E) (20, 31).

Next, we sought to verify that the antibody conjugated nanobins are specific for u-PAR expressing cells. To this end, the ES-2 OvCa cell line, which has high u-PAR expression (Fig. 1B), was infected with small hairpin (sh) RNAs against u-PAR. We found that shRNAs effectively knocked down u-PAR expression in ES-2 cells, and that the inhibition was preserved over several passages (Fig. 3A). Flow cytometry studies showed that uptake of ATN-291-NB(Calcein) was significantly lower in the u-PAR knock-down cells as compared to the wild-type cells (Fig. 3B), which was confirmed using confocal microscopy

(Fig. 3C). Moreover, addition of either the uPA antibody, ATN-291, or recombinant single chain uPA (scuPA) was able to dose-dependently compete out the cellular uptake of ATN-291-NB(Calcein) but did not affect the internalization of unconjugated NB(Calcein), either in HeyA8 (Fig. 3D) or ES-2 cells (Supplementary Fig. S1C, D) both of which express high uPA/u-PAR. These findings suggest that the delivery of ATN-291-nanobins is uPA and u-PAR-dependent.

Urokinase targeted arsenic loaded nanobins inhibit tumor growth

Next, we evaluated the efficacy of the ATN-291 decorated, arsenic trioxide loaded nanobins *in vitro* (Fig. 4) and *in vivo* (Fig. 5) to ascertain whether targeting nanobins with an antibody affects the delivery efficiency of the loaded arsenic. Cytotoxicity assays using HeyA8 cells were performed to determine if improved delivery would impact cell survival. At equivalent doses actively targeted ATN-291-NB(Ni,As) were more effective in suppressing cell survival of high uPA/u-PAR expressing HeyA8 cells than the unconjugated NB(Ni,As), as reflected by a significantly different IC_{50} (25 μM *versus* 53 μM, p=0.0002). In contrast, the low uPA/u-PAR expressing CaOV3 cells had a much higher IC_{50} (Supplementary Fig. S1E). In addition, ICP-MS analysis of cell fractions (cytosol, membrane/organelle, and nucleus) showed that targeted treatment with ATN-291 increased the intracellular delivery of arsenic by an average of 5.5 fold (Fig. 4A). More importantly, since a concern with nanobins has been that they can be trapped in endosomes and lysosomes (7, 8), only 13.9% of the arsenic was detected in the membrane/organelle fraction of ATN-291-NB(Ni,As). These results are consistent with the punctate, perinuclear fluorescence observed with ATN-291 nanobins (Fig. 2C, D).

Since As_2O_3 has been shown to induce apoptosis (33, 34), we first confirmed that free arsenic, NB(Ni,As), and ATN-291-NB(Ni,As) stimulate apoptosis by assessing nuclear fragmentation (Fig. 4B). ATN-291-NB(Ni,As) trigger early apoptosis, as evidenced by a loss in mitochondrial membrane potential ($\Delta\Psi_m$) which was confirmed both by confocal microscopy (Fig. 4C) and FACS analysis (Supplementary Fig. S2). We then assessed the effects of our nanobin preparations on the generation of cleaved caspase-3, a marker of caspase-dependent apoptosis. Figure 4D shows that both types of arsenic containing nanobins, as well as arsenic, induced caspase-3 cleavage in HeyA8 cells. The nanobin formulation significantly inhibited the expression of aldehyde dehydrogenase-1A1 (ALDH1A1), a marker of cancer stem cells (Fig. 4D) (35, 36). In contrast, conjugation with the antibody induced protein expression of both latent and active forms of the matrix metalloprotease (MMP)-2. This, however, did not affect MMP-2 activity of cancer cells treated with targeted or untargeted nanobins (Supplementary Fig. S3A). Given that uPA can convert plasminogen to plasmin, thereby generating proteolytic activity (19), we investigated the possibility that the targeted antibody might have activating functions. However, the targeted nanobins had no effect on plasminogen activation, invasion through collagen, or invasion in a 3D culture (27) of human omentum (Supplementary Fig. S3B–D).

Since arsenic-loaded, uPA targeted nanobins increased cytotoxicity and apoptosis *in vitro*, we studied their therapeutic effect (Fig. 5A–D) and biodistribution (Fig. 5E, F) *in vivo*. ATN-291-NB(Ni,As) treatment was tested in a human OvCa xenograft model in which HeyA8 OvCa cells were injected intraperitoneally (i.p.) into female nude mice (20). Four days post injection, mice were randomized to five groups and treated i.p. every other day with either PBS, ATN-291-NB(NaCl), As2O3, untargeted arsenic encapsulated nanobins NB(Ni,As), or targeted ATN-291-NB(Ni,As) at an As2O3 concentration of 4 mg/kg (14). All treated mice continued to gain weight and there was no apparent toxicity in any treatment group (Fig. 5A). Free As_2O_3, empty nanobins NB(NaCl) and PBS treatment had no impact on tumor growth (Fig. 5B), as reported by us previously in a breast cancer model

(14). NB(Ni,As) reduced tumor weight significantly and this effect was further enhanced with the addition of active targeting on the nanobins (Fig. 5B, C). Analysis of three independent xenograft experiments showed that, compared to the control treatment group, tumor weight was reduced by 27% (p=0.04) with the non-targeted NB(Ni,As) treatment and 47% (p=0.0005) with the targeted ATN-291-NB(Ni,As) treatments (Fig. 5C). The additional decrease in tumor burden after treatment with ATN-291-NB(Ni,As), compared to treatment with NB(Ni,As), was statistically significant (p=0.02).

Pathologic review of the tumors at the end of treatment showed undifferentiated, high grade tumors (Fig. 5D) which did not differ in angiogenesis (microvessel density, CD31), proliferation rate (Ki-67) (Supplementary Fig. S4), or u-PAR expression (data not shown). Both targeted and untargeted nanobins induced macrophage infiltration into the tumor. Untargeted nanobins recruited more macrophages than the uPA targeted nanobins (Supplementary Fig. S4). Treatment with the untargeted arsenic nanobins induced active caspase-3 and DNA fragmentation (TUNEL stain) in the tumors. These effects were more pronounced in ATN-291-NB(Ni, As) treated tumors (Fig. 5D), suggesting, as is consistent with the *in vitro* results (Fig. 4B–D), that arsenic-loaded nanobins reduce tumor burden by inducing apoptosis rather than by inhibiting tumor growth. Also consistent with the *in vitro* results is that ATN-291-NB(Ni,As) treatment reduced expression of ALDH1A1 (Fig. 4D) (35). Analysis of kidney and liver function in serum showed no significant toxicity with ATN-291-NB(Ni,As) treatment (Supplementary Fig. S5). Together, these results corroborate the therapeutic effectiveness of NB(Ni,As) treatment and the improved anti-tumoral effect of targeted ATN-291-NB(Ni,As) treatment.

To study biodistribution of nanobins using a fluorescence imaging system, HeyA8-GFP OvCa xenografts were established and then injected with nanobins. The ATN-291$_{AF647}$-NB(Ni,As) homed to the tumor, spleen, lung and liver (Fig. 5E), common accumulation sites for liposome nanoparticles (11, 37). *Ex vivo* images from ATN-291$_{AF647}$-NB(Ni,As) treated animals showed that the tumors had a higher fluorescence intensity than the organs, indicating the efficient delivery of nanobins to the tumor with active targeting. The arsenic concentration in organs/tumor detected by ICP-MS showed no significant difference in the total amount of As_2O_3 delivered to the tumors (Fig. 5F).

Discussion

Ovarian cancer is generally confined to the peritoneal cavity, and intraperitoneal chemotherapy treatment is a well-established clinical treatment modality (38). Therefore, nanoparticles that efficiently target tumor cells intraperitoneally, deliver anti-cancer drugs potently, and minimize the exposure of normal tissue to chemotherapeutics could lead to significant treatment improvements. Many reports show that the uPA system is consistently overexpressed in OvCa, and that its expression in normal cells is low (18, 20, 31). Given that the u-PAR is internalized upon uPA binding, we developed a uPA/u-PAR dependent targeted delivery using uPA antibody targeted nanobins.

We found that targeted single-agent treatment with nanobins (ATN-291-NB(Ni,As)) suppressed tumor growth in an orthotopic OvCa mouse model by almost 50%, while the untargeted NB(Ni,As), at equimolar arsenic doses, were half as effective (Fig. 5C). Several of our observations are consistent with the specific uptake of arsenic loaded nanobins by OvCa cells. When u-PAR expression was downregulated in cancer cells with shRNA, we observed reduced intracellular uptake of targeted nanobins (Fig. 3A–C). Consistent with this observation, confocal microscopy showed that the targeted nanobins were internalized (Fig. 2). Adding free antibody or competition with recombinant single-chain uPA to u-PAR

overexpressing cells also inhibited specific uptake of nanobins (Fig. 3D). Finally, the targeted nanobins were taken up *in vivo* by the uPA/u-PAR expressing tumor cells (Fig. 5E).

Antibodies are not the only targeting agents that can efficiently deliver intracellular payloads. We have previously shown that folate targeted liposomes containing arsenic trioxide are internalized by folate-receptor positive tumor cells but not by tumor cells without the receptor (12). In a different study, u-PAR targeted delivery of iron-oxide nanoparticles enhanced detection of human breast cancer using magnetic resonance imaging (39). Targeting transferrin nanoparticles not only delivered siRNA but allowed selective imaging of subcutaneous neuroblastoma tumors using a PET/CT scan (40). Conversely, targeting tumor vasculature using RGD-linked nanogels containing docetaxel inhibited tumor growth in a breast cancer model (41). These studies, together with our study, highlight the importance of specific intracellular delivery of payloads to achieve a therapeutic and diagnostic advantage.

Like integrin and folate receptors, the uPA/u-PAR is widely expressed in epithelial cancers. However unlike other receptors, their expression is found in tumor associated stromal cells as well as in tumor cells (18, 19). Further clinical development of this targeted nanomedicine hinges on leveraging uPA/u-PAR expression in tumor cells with this effective delivery system. A central challenge to clinical translation of targeted nanoparticles is the ability to reliably scale up and reproducibly characterize the drug carrier. The inclusion of antibodies to the nanobin surface, utilizing copper-catalyzed alkyne-azide cycloaddition click chemistry, has several advantages because it involves a reaction between alkyne and azide functional groups that are not otherwise found in biomolecules. Unlike other common conjugation methods using amine-coupling or thiol-coupling chemistries, this click reaction is chemically orthogonal to reactions that can occur between protein side chains, ensuring that no reactions occur that may lead to particle-particle crosslinking or non-specifically alter the surface properties of the nanobins. Additionally, the functional groups are not susceptible to hydrolysis. Click chemistry exposes only the thermally stable alkyne functional groups on the DSPE-PEG-Alkyne to high temperatures, avoiding thermal deactivation of the antibody. Since the ATN-291 antibody is labeled with AlexaFluor647 at a known ratio, we can use fluorophore concentration as a proxy for antibody concentration. Visible-light spectrometric measurements are subject to light-scattering interference in the presence of nanoparticles. By digesting the protein in a small sample of nanobins, then probing the liberated fluorophore after filtration of the liposomes, we can quantify the precise number of antibodies per particle without light-scattering interference from the lipid particles.

A landmark paper showed that arsenic trioxide is a very potent drug for the treatment of patients with acute promyelocytic leukemia (42). It is currently being considered for the treatment of solid human tumors because it has demonstrated potent cytotoxic effects against epithelial tumor cell lines *in vitro* (16). However, development in solid tumor indications has been limited by the poor pharmacokinetics and dose-limiting toxicity of the free drug. The most commonly described mechanisms of action (reviewed in (34)) of arsenic trioxide are inhibition of tumor angiogenesis, selective killing of cancer stem cells, inhibition of MMPs, and induction of apoptosis (14, 16, 17, 33). We found that ATN-291-NB(Ni,As) did not affect tumor cell proliferation or angiogenesis (Supplementary Fig. S4), but very efficiently induced OvCa cell apoptosis (Fig. 4B–D, 5D, Supplementary Fig. S2). This explained, at least in part, the observed significant cytotoxicity of the conjugated nanobins and is consistent with the mechanisms of arsenic function elucidated in a murine model of breast cancer (14). Liu *et al*. demonstrated that treatment with arsenic trioxide induced apoptosis and G_2/M cell cycle arrest in acute promyelocytic leukemia cells (33). This effect was more pronounced in leukemia cells with a mutated p53 gene, an observation

of potential significance for the treatment of OvCa since almost all serous OvCa have mutations within the p53 gene (43). We also showed inhibition of the cancer stem cell marker ALDH1A1 both *in vitro* and *in vivo* (Fig. 4D, 5D) by ATN-291-NB(Ni,As). These data are consistent with a study (36) reporting that ALDH1A1 is expressed in 73% of all human OvCa and that its silencing in OvCa cell lines blocked tumor cell growth *in vitro* and *in vivo*. The blocking of ALDH1A1 sensitized cells to platinum and taxane-based chemotherapy (36), which suggests that ATN-291-NB(Ni,As) may have a role in combination therapy for OvCa, since these tumors frequently develop chemotherapy resistance (1).

More than 60 years after the discovery of urokinase (44), the promise that tumor growth could be blocked by inhibiting specific proteases has not come to fruition. This is in part because other proteases compensate for the proteolytic function when a single protease is inhibited. However, given that most epithelial cancers strongly express uPA and u-PAR, it may be possible to harness the tumor associated uPA system as an entry point to deliver therapeutic or diagnostic payloads specifically to cancer cells rather than as a target for anti-proteolytic therapy. Although, in this report, we have focused on formulating As_2O_3 in a nanobin, our delivery system could also be loaded with other chemotherapeutics or imaging agents and employed to target any cancers that express uPA and u-PAR.

Supplementary Material

Refer to Web version on PubMed Central for supplementary material.

Acknowledgments

We thank the immunohistochemistry (Terri Li), light microscopy (Christine Labno), and electron microscopy (Yimei Chen) core facilities at the University of Chicago for their expert technical support. We want to acknowledge the help of Dr. Marion Curtis in analyzing the TCGA data and Gail Isenberg for carefully editing the manuscript. We thank the Integrated Molecular Structure Education and Research Center at Northwestern University for ICP-OES.

Grant support: This work was supported by NCI Alliance for Nanotechnology through a Cancer Nanotechnology Platform Partnership U01CA151461 (A.P. Mazar, E. Lengyel, T.V. O'Halloran), a National Science Foundation Graduate Research Fellowship Grant No. DGE-0824162 (P.L. Hankins), and a Clinical Translational Research Award from the Burroughs Wellcome fund (E. Lengyel). Arsenic biodistribution analysis was performed at the Northwestern University Quantitative Bioelemental Imaging Center generously supported by NASA Ames Research Center NNA06CB93G.

Abbreviations

AF647	AlexaFluor647
IP	intraperitoneally
AF647	AlexaFluor647
As2O3	arsenic trioxide
ATN-291	uPA antibody
DLS	dynamic light scattering
DSPC	1,2-distearoylsn-glycero-3-phosphocholine
DSPE-PEG	1,2-distearoyl-sn-glycero-3-phosphoethanolamine-N-[amino(polyethylene glycol]
ECM	extracellular matrix

FACS	Fluorescence activated cell sorting
ICP-MS	Inductively coupled plasma optical mass spectrometry
ICP-OES	Inductively coupled plasma optical emission spectrometry
MFI	Mean fluorescence intensity
NB	nanobin
OvCa	ovarian cancer
PDI	Polydispersity index
scuPA	single chain uPA
uPA	Urokinase plasminogen activator
u-PAR	uPA receptor
UV/Vis	ultraviolet–visible spectroscopy
ΔΨm	mitochondrial membrane potential.

References

1. Jelovac D, Armstrong DK. Recent progress in the diagnosis and treatment of ovarian cancer. CA Cancer J Clin. 2011; 61:183–203. [PubMed: 21521830]
2. Lengyel E. Ovarian cancer development and metastasis. Am J Pathol. 2010; 177:1053–1064. [PubMed: 20651229]
3. Vaughn S, Coward JI, Bast RC, Berchuck A, Berek JS, Brenton JD, et al. Rethinking ovarian cancer: Recommendations for improving outcomes. Nature Rev. 2011; 11:719–725.
4. Gabizon A, Shmeeda H, Barenholz Y. Pharmacokinetics of pegylated liposomal doxorubicin: Review of animal and human studies. Clin Pharmacokinet. 2003; 42:419–436. [PubMed: 12739982]
5. Gordon AN, Fleagle JT, Guthrie D, Parkin DE, Gore ME, Lacave AJ. Recurrent epithelial ovarian carcinoma: A randomized phase III study of pegylated liposomal doxorubicin versus topotecan. J Clin Oncol. 2001; 19:3312–3322. [PubMed: 11454878]
6. Vaage J, Donovan D, Mayhew E, Abra R, Huang A. Therapy of human ovarian carcinoma xenografts using doxorubicin encapsulated in sterically stabilized liposomes. Cancer. 1993; 72:3671–3675. [PubMed: 8252484]
7. Kim BY, Rutka JT, Chan WC. Nanomedicine. N Engl J Med. 2010; 363:2434–2443. [PubMed: 21158659]
8. Zamboni WC, Torchilin V, Patri AK, Hrkach J, Stern S, Lee R, et al. Best practices in cancer nanotechnology: Perspective from NCI nanotechnology alliance. Clin Cancer Res. 2012; 18:3229–3241. [PubMed: 22669131]
9. Kirpotin DB, Drummond DC, Shao Y, Shalaby MR, Hong K, Nielsen UB, et al. Antibody targeting of long-circulating lipidic nanoparticles does not increase tumor localization but does increase internalization in animal models. Cancer Res. 2006; 66:6732–6740. [PubMed: 16818648]
10. Salva R, Taratula O, Garbuzenko O, Minko T. Tumor targeted quantum dot-mucin 1 aptamer-doxorubicin conjugate for imaging and treatment of cancer. J Control Release. 2011; 153:16–22. [PubMed: 21342659]
11. Xiao K, Li Y, Lee JS, Gonik AM, Dong T, Fung G, et al. "OA02" peptide facilitates the precise targeting of paclitaxel-loaded micellar nanoparticles to ovarian cancer in vivo. Cancer Res. 2012; 72:2100–2110. [PubMed: 22396491]
12. Chen H, Ahn R, Van den Bossche J, Thompson DH, O'Halloran TV. Folate-mediated intracellular drug delivery increases the anticancer efficacy of nanoparticulate formulation of arsenic trioxide. Mol Cancer Ther. 2009; 8:1955–1963. [PubMed: 19567824]

13. Kirpotin DB, Noble CO, Hayes ME, Huang Z, Kornaga T, Zhou Y, et al. Building and characterizing antibody-targeted lipidic nanotherapeutics. Methods Enzym. 2012; 502:139–166.
14. Ahn RW, Chen F, Chen H, Stern ST, Clogston JD, Patri AK, et al. A novel nanoparticulate formulation of arsenic trioxide with enhanced therapeutic efficacy in a murine model of breast cancer. Clin Cancer Res. 2010; 16:3607–3617. [PubMed: 20519360]
15. Chen H, MacDonald R, Li S, Krett NL, Rosen ST, O'Halloran TV. Lipid encapsulation of arsenic trioxide attenuates cytotoxicity and allows for controlled anticancer drug release. J Am Chem Soc. 2006; 128:13348–13349. [PubMed: 17031934]
16. Uslu R, Sanli UA, Sezgin C, Karabulut B, Terzioglu E, Omay SB, et al. Arsenic trioxide-mediated cytotoxicity and apoptosis in prostate and ovarian carcinoma cell lines. Clin Cancer Res. 2000; 6:4957–4964. [PubMed: 11156257]
17. Zhang J, Wang B. Arsenic trioxide (As2O3) inhibits peritoneal invasion of ovarian carcinoma cells in vitro and in vivo. Gynecol Oncol. 2006; 103:199–206. [PubMed: 16624393]
18. Mazar AP, Ahn RW, O'Halloran TV. Development of novel therapeutics targeting the urokinase plasminogen activator receptor (uPAR) and their translation toward the clinic. Curr Pharm Des. 2011; 17:1970–1978. [PubMed: 21711234]
19. Mazar AP. Urokinase plasminogen activator receptor choreographs multiple ligand interactions: Implications for tumor progression and therapy. Clin Cancer Res. 2008; 14:5649–5655. [PubMed: 18794071]
20. Kenny HA, Leonhardt P, Ladanyi A, Yamada SD, Montag AG, Im HK, et al. Targeting the urokinase plasminogen activator receptor inhibits ovarian cancer metastasis. Clin Cancer Res. 2011; 17:459–471. [PubMed: 21149615]
21. Cubellis M, Wun T, Blasi F. Receptor-mediated internalization and degradation of urokinase is caused by its specific inhibitor PAI-1. EMBO J. 1990; 9:1079–1085. [PubMed: 2157592]
22. Conese M, Nykjaer A, Petersen CM, Andreasen PA, Gliemann J, Christensen EI, et al. α-2 Macroglobulin receptor/LDL receptor-related protein (Lrp)-dependent internalization of the urokinase receptor. J Cell Biol. 1995; 131:1609–1622. [PubMed: 8522616]
23. Kaur S, Kenny HA, Jagadeeswaran S, Zillhardt M, Montag AG, Kistner E, et al. β3-integrin expression on tumor cells inhibits tumor progression, reduces metastasis, and is associated with a favorable prognosis in patients with ovarian cancer. Am J Pathol. 2009; 175:2184–2196. [PubMed: 19808644]
24. Hong V, Presolski SI, Ma C, Finn MG. Analysis and optimization of copper-catalyzed azide-alkkyne cycloaddition for bioconjugation. Angewandte Chem. 2009; 121:10063–10067.
25. Nieman KM, Kenny HA, Penicka CV, Ladanyi A, Buell-Gutbrod R, Zillhardt M, et al. Adipocytes promote ovarian cancer metastasis and provide energy for rapid tumor growth. Nature Med. 2011; 17:1498–1503. [PubMed: 22037646]
26. Sawada K, Radjabi AR, Shinomiya N, Kistner E, Kenny HA, Salgia R, et al. C-Met overexpression is a prognostic factor in ovarian cancer and an effective target for inhibition of peritoneal dissemination and invasion. Cancer Res. 2007; 67:1670–1680. [PubMed: 17308108]
27. Kenny HA, Krausz T, Yamada SD, Lengyel E. Use of a novel 3D culture model to elucidate the role of mesothelial cells, fibroblasts and extra-cellular matrices on adhesion and invasion of ovarian cancer cells. Int J Cancer. 2007; 121:1463–1472. [PubMed: 17546601]
28. Mitra AK, Zillhardt M, Hua YJ, Tiwari P, Murmann A, Peter ME, et al. MicroRNAs reprogram normal fibroblasts into cancer-associated fibroblasts in ovarian cancer. Cancer Discov. 2012; 2:1100–1108. [PubMed: 23171795]
29. The Cancer Genome Atlas Network. Integrated genomic analyses of ovarian carcinoma. Nature. 2011; 474:609–615. [PubMed: 21720365]
30. Cerami E, Gao J, Dogrusoz U, Gross BE, Sumer S, Arman B, et al. The cBio cancer genomics portal: An open platform for exploring multidimensional cancer genomics data. Cancer Discov. 2012; 2:401–404. [PubMed: 22588877]
31. Al-Hassan NN, Behzadian A, Caldwell R, Ivanova VS, Syed V, Motamed K, et al. Differential roles of uPAR in peritoneal ovarian carcinomatosis. Neoplasia. 2012; 14:259–270. [PubMed: 22577342]

32. Vermeer W, Norde W. The thermal stability of immunoglobulin: Unfolding and aggregation of a muti-domain protein. Biophys J. 2000; 78:394–404. [PubMed: 10620303]
33. Liu Q, Hilsenbeck S, Gazitt Y. Arsenic trioxide-induced apoptosis in myeloma cells: p53-dependent G1 or G2/M cell cycle arrest, activation of caspase-8 or caspase-9, and synergy with AP02/TRAIL. Blood. 2003; 101:4078–4087. [PubMed: 12531793]
34. Miller WH, Schipper HM, Lee JS, Singer J, Waxman S. Mechanisms of action of arsenic trioxide. Cancer Res. 2002; 62:3893–3903. [PubMed: 12124315]
35. Chenna V, Hu C, Pramanik D, Aftab BT, Karikari C, Campbell NR, et al. A polymeric nanoparticle encapsulated small-molecule inhibitor of hedgehog signaling (nanoHHI) bypasses secondary mutational resistance to smoothened antagonists. Mol Cancer Ther. 2011; 11:165–173. [PubMed: 22027695]
36. Landen CN, Goodman B, Katre AA, Steg AD, Nick AM, Stone RL, et al. Targeting aldehyde dehydrogenase cancer stem cells in ovarian cancer. Mol Cancer Ther. 2010; 9:3186–3199. [PubMed: 20889728]
37. Dadashzadeh S, Mirahmadi N, Babaei MH, Vali AM. Peritoneal retention of liposomes:Eeffects of lipid composition, PEG coating and lipsome charge. J Control Release. 2010; 148:177–186. [PubMed: 20800629]
38. Armstrong DK, Bundy B, Wenzel L, Huang H, Baergen R, Lele S, et al. Intraperitoneal cisplatin and paclitaxel in ovarian cancer. N Engl J Med. 2006; 353:34–43. [PubMed: 16394300]
39. Yang L, Peng XH, Wang X, Cao Z, Ni C, Karna P, et al. Receptor-Targeted nanoparticles for in vivo imaging of breast cancer. Clin Cancer Res. 2009; 15:4722–4732. [PubMed: 19584158]
40. Barlett DW, Su H, Hildebrandt IJ, Weber WA, Davis ME. Impact of tumor-specific targeting on the biodistribution and efficacy of siRNA nanoparticles measured by multimodality and vivo imaging. Proc Natl Acad Sci USA. 2007; 104:15549–15554. [PubMed: 17875985]
41. Murphy EA, Majeti BK, Mukhavaram R, Acevedo LM, Barnes LA, Cheresh D. Targeted nanogels: A versatile platform for drug delivery to tumors. Mol Cancer Ther. 2011; 10:972–982. [PubMed: 21518727]
42. Soignet SL, Maslak P, Wang ZG, Jhanwar S, Calleja E, Dardashti LJ, et al. Complete remission after treatment of acute pro-myelocytic leukemia with arsenic trioxide. N Engl J Med. 1998; 339:1341–1348. [PubMed: 9801394]
43. Ahmet AA, Etemadmoghadam D, Temple J, Lynch AG, Riad M, Sharma R, et al. Driver mutations in TP53 are ubiquitous in high grade serous carcinoma of the ovary. J Pathology. 2010; 221:49–56.
44. MacFarlane RG, Pilling J. Fibrinolytic activity of normal urine. Nature. 1947; 159:779. [PubMed: 20241608]

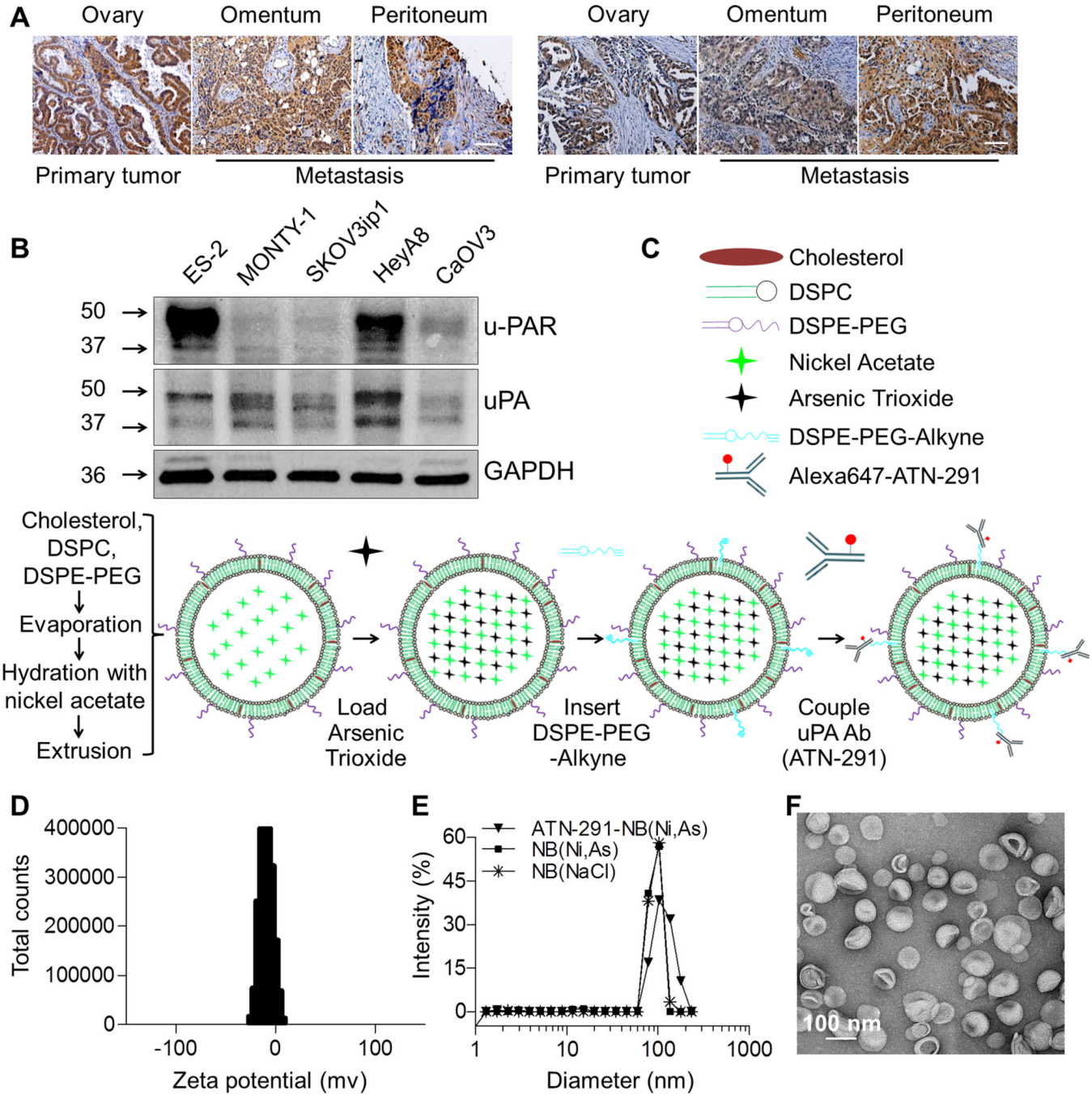

Figure 1. Urokinase receptor (u-PAR) targeting nanobins to treat ovarian cancer

A, Immunohistochemical images of u-PAR expression in primary (ovary) and metastatic (omentum, peritoneum) serous-papillary OvCa in two representative patients. Scale bar, 200 μm.

B, Immunoblot analysis of u-PAR and urokinase (uPA) expression in human OvCa cell lines (ES-2, SKOV3ip1, HeyA8 and CaOV3) and a primary OvCa clone, MONTY1.

C, Schematic of nanobin synthesis. Arsenic trioxide (As) co-precipitated with nickel actate (Ni) inside nanobins (NBs) which were sequentially conjugated with uPA antibody (ATN-291) to target OvCa cells expressing u-PAR.

D, Zeta potential distribution of ATN-291-NB(Ni,As).
E, Hydrodynamic sizes of ATN-291-NB(Ni,As)(▼), NB(Ni,As)(■), and NB(NaCl)(*) were measured by dynamic light scattering.
F, Transmission electron micrograph of ATN-291-NB(Ni,As) stained with 1% uranyl acetate. Scale bar, 100 nm.

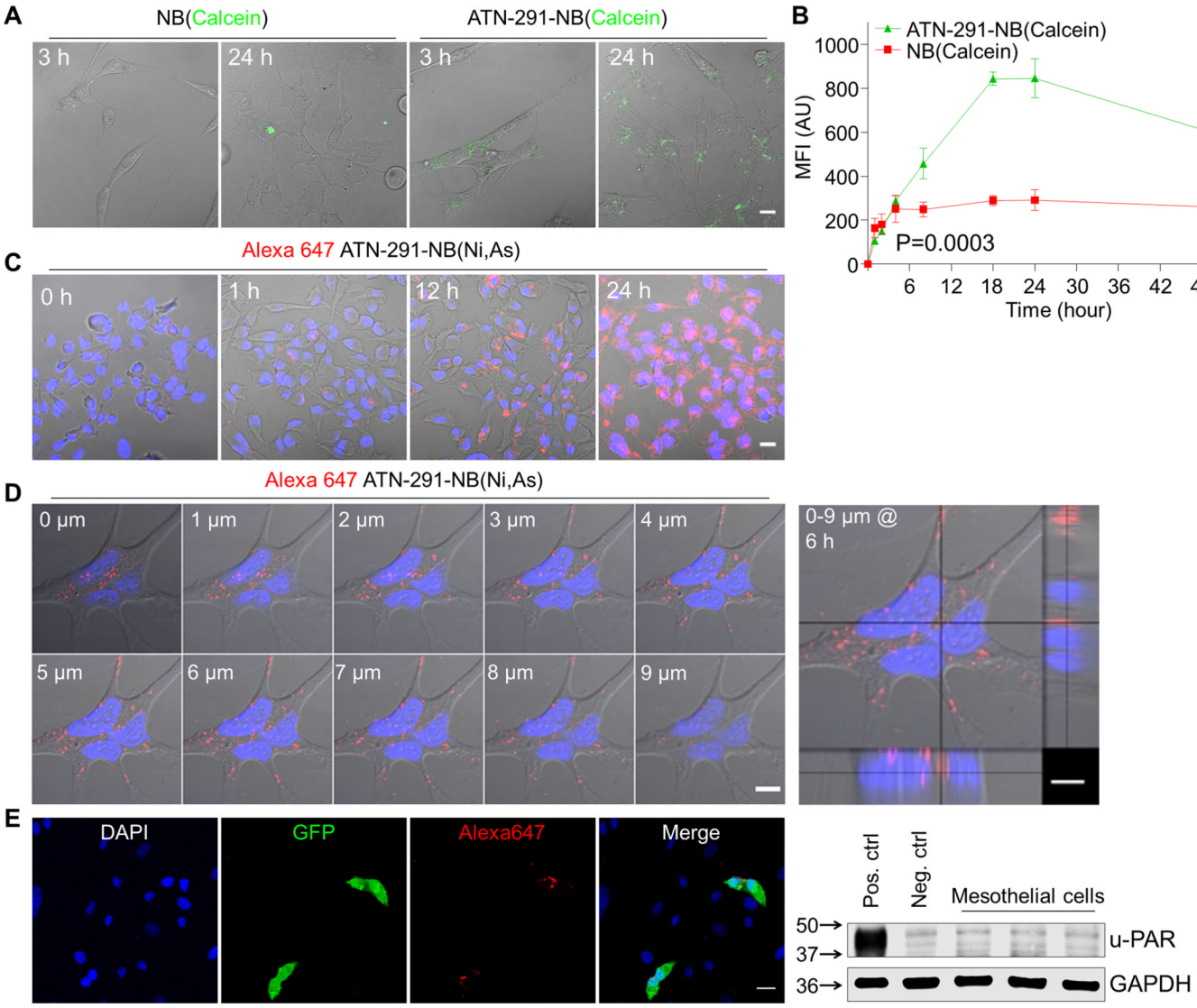

Figure 2. Fluorescence analysis of nanobin (NB) uptake in ovarian cancer cells

A, Confocal microscopy of HeyA8 OvCa cells treated with ATN-291 conjugated and unconjugated NB(Calcein) for 3 h and 24 h. Scale bar, 20 µm.

B, Flow cytometry. Comparison of cellular uptake of ATN-291 conjugated (▲) or unconjugated (■) NB(Calcein) in HeyA8 cells over time (1–48 h). Bars represent means ± SEM from 3 independent experiments. Statistical analyses were performed using two-way ANOVA. MFI, mean fluorescence intensity.

C–D, Confocal microscopy analyses of HeyA8 OvCa cells treated with Alexa647 labeled ATN-291-NB(Ni,As). (**C**) Time course (0–24 h). Merged pictures of Alexa647 (red), Hoechst (nucleus, blue) and differential interfering contrast images are shown. (**D**) Z-axis (0–9 µm) reconstruction of optical sections with orthogonal views (right) after 6 h of treatment. Scale bar, 20 µm.

E, Tumor cell–targeted nanobin delivery. Human primary omental mesothelial cells were co-cultured with GFP labeled HeyA8 and treated with ATN-291$_{AF647}$-NB(Ni,As) for 24 h before confocal imaging. Nuclei were counterstained with DAPI. Scale bar, 20 µm. Immunoblot analysis of u-PAR expression in human primary mesothelial cells from three

OvCa patients (right). u-PAR expressing ES-2 cells and ES-2 cells stably transfected with a shRNA targeting u-PAR serve as positive and negative controls, respectively.

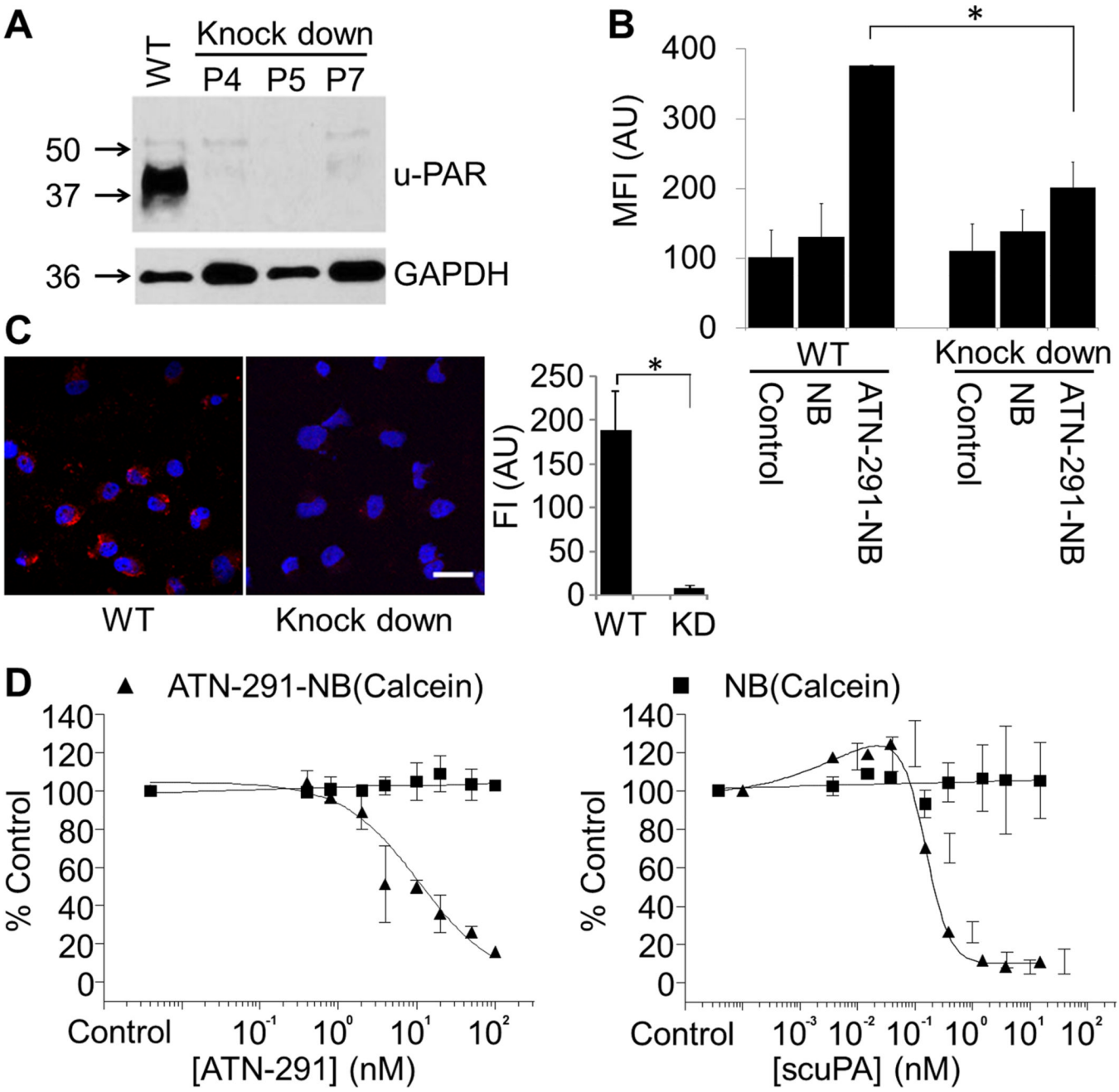

Figure 3. Cellular uptake of urokinase antibody (ATN-291) conjugated nanobin (NB) is u-PAR dependent

A, Immunoblot analysis of u-PAR expression in wild-type (WT) and u-PAR shRNA stably-expressing (knock down, KD) ES-2 OvCa cells (passage number, P).

B, Flow cytometry of NB(Calcein) and ATN-291-NB(Calcein) uptake in ES-2 WT and KD cells (24 h). Control, no treatment. *, p value< 0.05. Bars represent means ± SEM from 3 independent experiments. Statistical analyses were performed using a two-tailed *t*-test.

C, Confocal microscopy analysis of Alexa647 (Red) labeled ATN-291-NB(NaCl) uptake in ES-2 WT and KD cells (24 h). Merged pictures of Alexa647 (red) and Hoechst (nucleus, blue) are shown. Scale bar, 20 μm. Quantification of AF647 fluorescence intensity (right).

D, Competition assays. HeyA8 cells were pre-treated with the indicated concentrations of uPA antibody ATN-291 (left) or with the single chain uPA (scuPA) (right). Subsequently 25 μM of ATN-291-NB(Calcein ▲), or as control NB(Calcein ■) was added for 24 h and cells analyzed by flow cytometry. The results were normalized to cells without ATN-291 or scuPA treatment. Bars represent means ± SEM from 3 independent experiments.

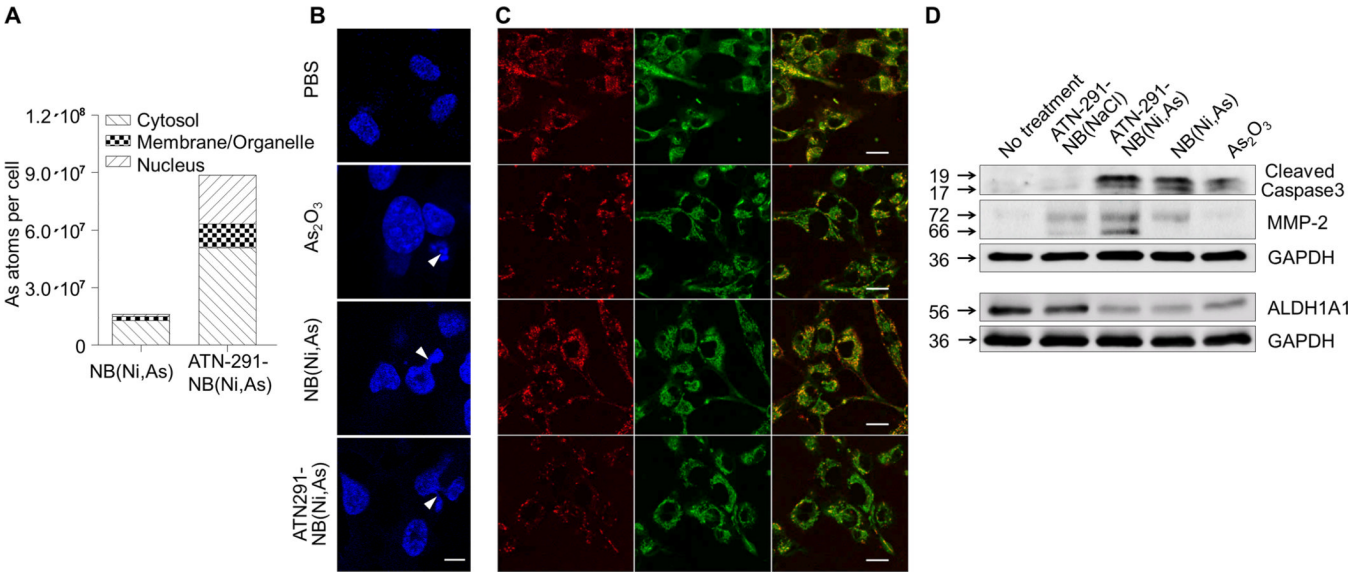

Figure 4. The cytotoxicity of NB(Ni,As) is increased after conjugation with uPA antibody (ATN-291)

A, ICP-MS analysis of arsenic (As) content in cell compartments. After incubation with ATN-291-NB(Ni,As) or NB(Ni,As) for 24 h, HeyA8 cells were fractionated into cytosol, membrane/organelles, and nuclear compartments which were then analyzed for arsenic content by ICP-MS. The numbers of arsenic atoms were normalized to the empty nanobin (NB(NaCl)) control.

(**B,C**) Confocal microscopy. HeyA8 cells were treated with either PBS (control), arsenic trioxide, NB(Ni,As), or ATN291-NB(Ni,As) ([As] = 25 μM) for 18 h (B), or 2 h (C). (**B**) Nuclear fragmentation was visualized using Hoechst staining. Fragmented nuclei are highlighted with white arrow heads. Scale bar, 10 μm. (**C**) Mitochondrial membrane potential (ΔΨm). Cells were stained with the membrane-permeant dye JC-1 (2 μM) which undergoes an emission shift from red to green fluorescence when cells lose ΔΨm: JC-1 emits red fluorescence (590nm) in polarized mitochondrial membranes; while it fluoresces green (529 nm) in the cells with depolarized mitochondrial potential, a trait of early apoptosis. Scale bar, 20 μm.

D, Immunoblot analysis of MMP-2, ALDH1A1, and cleaved caspase-3 expression in HeyA8 cells after treatment for 1 day. GAPDH was used as an internal control.

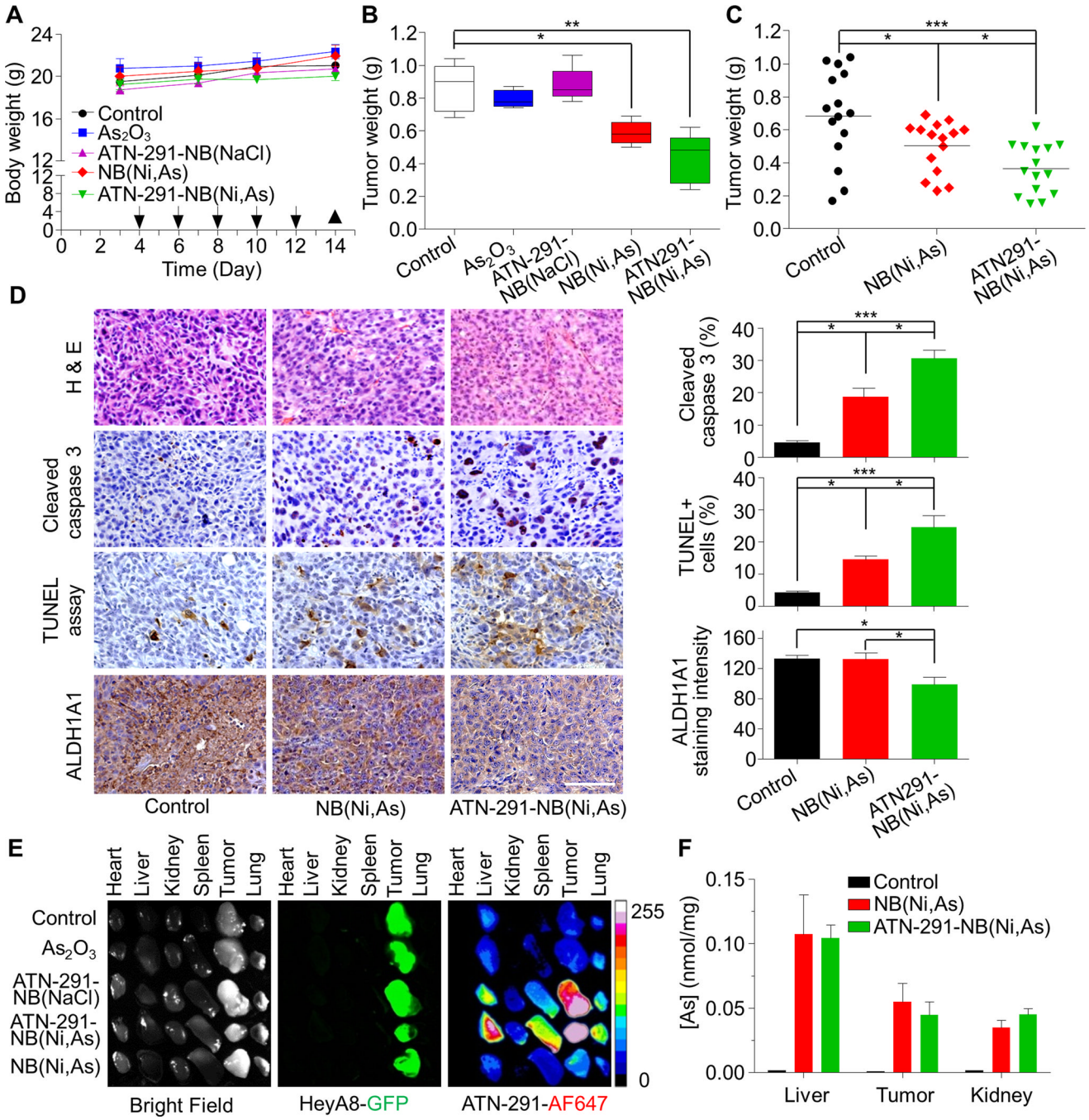

Figure 5. Arsenic (As)-loaded nanobin (NB) reduced tumor burden in an ovarian cancer xenograft mouse model

A, Body weight and treatment timeline. HeyA8-GFP OvCa cells were injected i.p. into female nude mice. The NB(Ni,As), ATN-291-NB(Ni,As) (4 mg/kg, As) or control treatments (PBS, As_2O_3, or ATN-291-NB(NaCl)) were also i.p. injected (arrow) (5 mice/group). Tumors were collected on day 14 (▲).

B, Tumor weight of each treatment group. The bottom and top of the box are the 25th and 75th and the line in the middle is the median. The whiskers are the minimum and maximum value.

C, Effect of targeted ATN-291-NB(Ni,As) and untargeted nanobins NB(Ni,As) on tumor weight at the end of treatment of HeyA8-GFP OvCa xenografts-3 independent studies, n=15 mice.
D, Hematoxylin and eosin staining and immunohistochemistry for cleaved caspase-3, ovarian stem cell marker (ALDH1A1) and TUNEL staining. Scale bar, 100 μm. Quantification of ALDH1A1, cleaved caspase 3 positive cells and percentage of TUNEL-positive cells over total tumor cells (right). Columns represent means ± SEM. *** $p<0.001$;** $p<0.01$; * $p<0.05$. Statistical analyses were performed using two-tailed *t*-test.
E, Individual organs (i.e. heart, liver, kidney, spleen, lung) and tumors were dissected on day 14 and imaged for fluorescence using an OV100 Olympus fluorescence molecular imaging systems. The HeyA8-GFP OvCa cells are green and the uPA-targeted nanobins are red (Alexa647).
F, The same experiment as in D was repeated and arsenic (As) concentration quantified using ICP-MS (n=6 mice).

Table 1

Nanobin concentrations, size, polydispersity index, and zeta potential

Nanobin	Concentration (mM)				Size (nm)[c]	Polydispersity Index[c]	Zeta Potential (mV)
	[As][a]	[Ni][a]	[Lipid][a]	Antibody[b]			
NB(Ni,As)	8.8±0.6	10.4±0.7	18.2±1.3	-	94.4±1.7	0.05±0.01	−2.14
ATN-291-NB(Ni,As)	8.5±0.3	10.7±0.2	18.7±1.4	8.5±1.2	104.5±3.1	0.10±0.02	−3

[a] Measured by inductively-coupled plasma optical emission spectroscopy

[b] Quantification of cleaved Alexa647-labeled urokinase antibody using a fluorescence spectrophotometer

[c] Measured by dynamic light scattering